JP&M Engineering
Journal of Petroleum and Mining Engineering

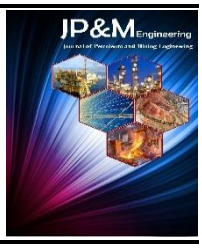

Phosphate-doped polyaniline/silica dust composite coatings of stainless steel for protection against corrosion

Atef.E. Mahmoud,*[a] Abou-Elhagag A. Hermas[b] and Eatemad M.Ahmed[b]
[a]Mining & Metallurgical Engineering Department, Faculty of Engineering, Assiut University
[b]Department of Chemistry, Faculty of Science, Assiut University, Assiut, Egypt
*Corresponding author: atef66@aun.edu.g

Article Info

Received 21 Jul. 2024
Revised 24 Nov. 2024
Accepted 10 Dec. 2024

Keywords

coating, corrosion, electropolymerization, polyaniline, silica dust,"

Abstract

Polyaniline (PANI) and its composites are promising protective coatings for corrosion control of steel materials. A PANI/silica nanocomposite coating, containing silica nanoparticles (93.5% SiO_2), was electrodeposited onto stainless steel (SS) from a sulfuric acid solution using cyclic voltammetry. The coating was characterized using various techniques, including Fourier-transform infrared spectroscopy (FTIR), energy-dispersive X-ray analysis (EDX), X-ray powder diffraction (XRD), scanning electron microscopy (SEM), thermal analysis, water sorption (WS%) testing, and electrochemical measurements. The addition of silica nanoparticles decreased the electrodeposition rate, altered the structure, improved thermal stability, and reduced WS%. The optimal nanoparticle concentration for achieving the highest protective performance was found to be 0.04 g of silica per 100 mL of solution. Phosphate anions were incorporated into the PANI molecules by aging the coated steel in a phosphate solution. The coated SS exhibited spontaneous passivation in a 3.5% NaCl solution, maintaining its protective properties for a specific period before breakdown. Notably, phosphating the PANI/silica coatings for more than three days prevented passivity breakdown for up to 350 hs. The underlying oxide layer formed beneath the coating, which varies depending on the coating type, plays a crucial role in protection against pitting corrosion.

Introduction

Pitting corrosion is one of several forms of corrosion that can cause severe and costly damage to stainless steel substrates. Its occurrence and associated costs are difficult to eliminate from both economic and environmental perspectives [1]. The rapid penetration of aggressive ions, such as chloride, creates deep pits that often go undetected. As these pits continue to grow, they can perforate the metal substrate [2].

Superhydrophobic coatings, which repel water and corrosive ions, play a significant role in corrosion prevention. Conducting polymer coatings offer protection by inhibiting and slowing down corrosion [3, 4]. Among these, PANI is a promising conducting polymer coating due to its favorable electronic properties, stability against environmental degradation, and ease of production. PANI is also considered an effective alternative to toxic chromium-based coatings [5, 6]. PANI and its composites protect metal substrates through barrier and anodic protection, performing well in both alkaline and acidic solutions [7-9]. The dense, adherent, and low-porosity passive film formed at the metal/coating interface acts as an impervious barrier, preventing penetration of aggressive anions and thereby inhibiting corrosion [10-12].

There are two main perspectives on the nature of the passive layer formed by PANI: (a) a metal oxide/hydroxide layer, attributed to the redox capability of PANI [10-13], and (b) a metal salt layer formed from reactions between metal cations and dopant anions [14-18]. Similar to chromate, PANI is redox-active, with equilibrium potentials more positive than those of commonly used metals, enabling it to provide anodic protection. It is believed that PANI restricts electron transfer from the metal to oxidizing agents.

PANI can be electrochemically synthesized by cyclic voltammetry, in which PANI is deposited from a monomer solution onto a conductive substrate as the monomer undergoes oxidation, triggering polymerization [19-21]. The size of the counter-anion dopant significantly influences the corrosion protection performance of PANI coatings: larger anions are less likely to be displaced by external aggressive anions like chloride, while smaller dopant

anions are more mobile and can be readily exchanged [19]. The incorporation of nanoparticles into the PANI matrix enhances the physical and adhesive properties of the coating, making polymer nanocomposites highly effective for corrosion protection. Examples include PANI-TiO_2 nanocomposites [22, 23], polymer–carbon nanotube composites [24, 25], and polymer–Al_2O_3 nanocomposites [26].

This study aims to investigate the protection of stainless steel against pitting corrosion in chloride solutions using an electrodeposited phosphate-doped PANI/silica composite.

Experimental

Materials

Aniline was purchased from Sigma–Aldrich and distilled prior to use. Sulfuric acid, sodium chloride, and sodium phosphate were obtained from BDH Chemicals, while silica dust nanoparticles (93.5% SiO_2) were supplied by Egyptian Ferroalloys Co. Ortho-chloroaniline was sourced from Alpha Aesar. Austenitic stainless steel 304, with a surface area of 0.23 cm^2 (chemical composition in Table 1), was used as the working electrode. The electrode was polished with abrasive paper up to 400 grit, then rinsed with double-distilled water and acetone. A platinum sheet served as the counter electrode, and an Ag/AgCl electrode in 3M KCl was used as the reference electrode. Double-distilled water was used for the preparation of all electrolytes employed during the electrodeposition process and electrochemical measurements.

Table (1) Chemical composition (wt. %) of stainless steel sample.

Cr	Mn	Si	Ni	Mo	C	P	Cu	Fe
18.15	2.23	0.26	8.78	0.08	0.31	0.06	0.25	69.87

Electro-deposition of PANI layer

PANI was electrodeposited onto 304 stainless steel (SS) using cyclic voltammetry in an aqueous solution of 1 M sulfuric acid containing 0.1 M aniline. The potential was scanned from -0.3 V to +1.1 V (versus Ag/AgCl in KCl) at a scan rate of 50 mV/s, with a Pt mesh as the counter electrode. Ortho-chloroaniline was used as an adhesion promoter prior to the coating process. The electrodeposition of the PANI/silica nanocomposite coating was performed with varying silica nanoparticle contents (0.02–0.1 g silica) suspended in the acidic electrolyte solution. To replace the sulfate counter-ions in PANI with larger phosphate anions, some PANI-coated steel samples were immersed in 0.1 M sodium phosphate tribasic solution at room temperature for different durations.

Characterizations

The characteristic structures of silica nanoparticles, PANI, and PANI/silica composites were investigated using FTIR (Nicolet iS10) in the range of 4000–500 cm^{-1}. The morphology of the deposited polymer layers and oxide films on the SS electrodes was examined using a JEOL JSM 5400LV scanning electron microscope (SEM). The SS electrodes were etched for 1 minute in an aggressive mixture of nitric acid (10 mL), acetic acid (10 mL), hydrochloric acid (15 mL), and glycerin (3 drops). Energy dispersive X-ray analysis (EDX) provided valuable information on the chemical composition of both the coated and corroding surfaces of the SS samples.

X-ray powder diffraction (XRD) patterns of the deposited films were obtained using a Philips type XRD diffractometer, model PW 1710, with a copper anode and a graphite monochromator (λ = 1.541838 Å). The generator was operated at 40 kV and 30 mA, with the diffractometer set to 2θ, using diverging and receiving slits and a step time of 10 $minutes^{-1}$. The peak intensity is correlated with the concentration of atoms or metal ions. Thermal analysis of the polymer-deposited films was conducted using a DTG-60H Simultaneous DTA-TG apparatus (Shimadzu). Thermal analysis experiments were performed to evaluate the thermo-oxidative stability of the nanocomposites and investigate the effects of nanoparticle incorporation.

Water sorption percentage

Water sorption percentage (WS%) was calculated by immersing the coated composites in a sodium chloride solution using the gravimetric method. The coated sheet samples (~12 cm^2) were weighed before immersion (W_o) and at various time intervals (W) at 40°C and 70°C. After immersion, the samples were removed, and surface water was wiped off with a dry cloth before immediate weighing to determine the weight (W). The percentage increase in weight was calculated to the nearest 0.1% using the formula ($W - W_o$) / W_o [27].The WS% at a given time can be calculated from the equation (1)

$$W_S = \frac{W - W_o}{W_o} \times 100 \quad (1)$$

Electrochemical corrosion measurements

Electrochemical studies, including open circuit potential (OCP) versus time measurement, anodic polarization, and electrochemical impedance spectroscopy (EIS), were performed in a 3.5% NaCl solution on both uncoated and coated SS samples. The anodic polarization curves were measured by varying the electrode potential between 0 V and +1.7 V from the OCP at a scan rate of 0.25 mV/s. Electrochemical impedance measurements were recorded over a frequency range of 10^5–0.5 Hz, with 10 points per decade, and a signal amplitude of 5 mV at OCP. Impedance spectra were analyzed by fitting the experimental results to equivalent circuits using the Zsim software.

This section may be divided by subheadings. You can apply “Heading2 and Heading 3” if needed. It should provide a concise and precise description of the experimental results, their interpretation as well as the experimental conclusions that can be drawn. Authors should discuss the results and how they can be interpreted in perspective of previous studies and of the working hypotheses. The findings and their implications should be discussed in the broadest context possible. Future research directions may also be highlighted.

Results and discussion

Electrochemical synthesis of PANI/silica composite coatings

Since the dissolution of oxidizable metals, like iron, occurs at a lower potential than that of the monomer oxidation potential, the metal must be passivated to create a suitable surface prior to the electropolymerization of electroactive specimens. Therefore, the SS is immersed in ortho-chloro-aniline before the coating procedures [12]. When the pre-treated bare SS is immersed in the electrolyte solution, the potential spontaneously shifts to the passive region of SS, forming a passive surface film. This film facilitates monomer oxidation, promoting polymer formation [28-30]. Electrodeposition of PANI on passivated stainless steel by cyclic voltammetry (CV) is shown in Fig. 1. The current response increases with successive potential scans, indicating the growth of the electroactive PANI film on the stainless steel surface. At the end of the experiment, a thick green layer is obtained on the SS substrate, which corresponds to the formation of emeraldine salt, the conductive form of PANI [24].

Electrodeposition of the PANI/silica composite is achieved by adding silica dust nanoparticles to the electrolyte solution. Figure 2 shows the 20th cycle of the CVs for PANI electrodeposition in the presence of silica dust nanoparticles at concentrations of 0.02–0.1 g/100 ml. The CVs show lower redox current density values compared to neat PANI, indicating that silica dust nanoparticles inhibit aniline monomer oxidation, thereby decreasing the amount of deposited polymer. Electrochemical measurements reveal that the highest protective composites were obtained with 0.04 g of silica dust nanoparticles, resulting in the most adherent PANI layer.

The coulombic charge (Q) for PANI electrodeposition was calculated by integrating the anodic peak of each cycle. The thickness of the deposited PANI layer was calculated using Equation (2) [18].

$$d = \frac{QM}{nFA\rho} \quad (2)$$

Where d is the thickness of the deposited PANI layer, Q is the total charge of the deposited polymer, M is the molecular weight of aniline, n is number of electrons/aniline, A is the area of the electrode, ρ is the specific density of aniline and F is the Faraday’s constant. Results show that the PANI thickness on the SS surface decreases with increasing silica content, yielding layer thicknesses of 9.94, 7.65, 3.66, and 1.41 µm in the presence of 0.0, 0.02, 0.04, and 0.06 g of silica particles, respectively. As illustrated in Fig. 3, the deposition rate of PANI gradually decreases with increasing silica dust content in the deposition bath. Consequently, the amount of deposited PANI and the thickness of the layer decrease as the silica concentration increases.

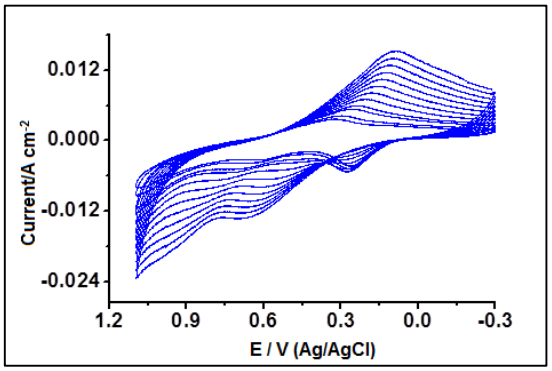

Figure 1 Cyclic voltammograms of an SS electrode recorded successively in a 1 M H_2SO_4 solution containing 0.1 M aniline monomer.

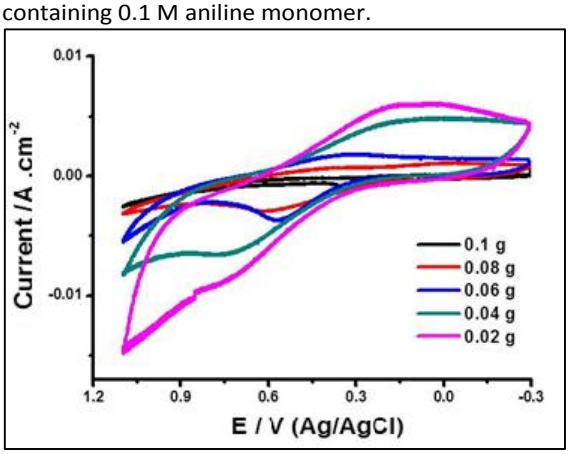

Figure 2 Comparative CVs (20th cycle) of SS electrode in 1M H_2SO_4 containing 0.1M ANI monomer with varying silica dust particle concentrations.

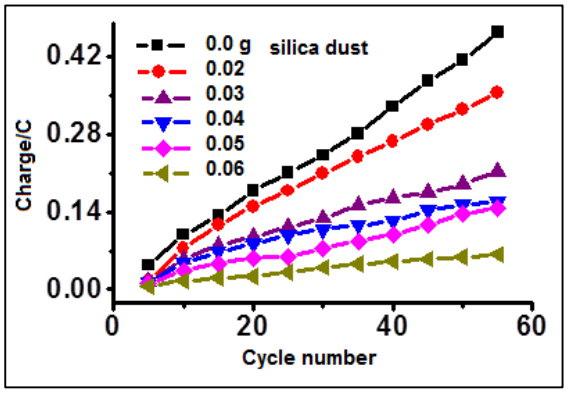

Figure 3 Influence of silica dust content on the electro-deposition rate of PANI on SS electrode.

Investigation of PANI layers

The FTIR spectra of silica dust particles, PANI, and PANI/silica coatings are shown in Figure 4. The spectrum of silica nanoparticles (Fig. 4a) displays a peak at a wavenumber of 1080 cm^{-1}, associated with the SiO_2 group [31, 32]. The FTIR spectra of PANI and PANI/silica coatings (Fig. 4b) exhibit two peaks at 3435.7 cm^{-1} and 2926.3 cm^{-1}, corresponding to the N-H stretching vibration in PANI. A peak at 1560.2 cm^{-1} represents the C=N stretching vibration of the quinonoid ring, while a peak at 1476.75 cm^{-1} corresponds to the C-C aromatic bond. Peaks at 1300.6 cm^{-1} and 1236.6 cm^{-1} are attributed to C-N stretching vibrations in the QBQ structure (Q = quinoid unit, B = benzenoid unit), while peaks at 1143.4 cm^{-1} and 1068.5 cm^{-1} are due to C-H bending in the quinoid structure. The peaks at 882.6 cm^{-1}, 849.9 cm^{-1}, and 709.1 cm^{-1} indicate aromatic C-H bending out of plane [26, 30, 33]. These findings confirm that electrochemical polymerization of aniline occurred, leading to the deposition of a PANI coating.

In the spectrum of the PANI/silica coating shown in Fig. 4b, all peaks corresponding to PANI are present. Additionally, the PANI-silica nanocomposite spectrum displays two new absorption peaks at 1070 cm^{-1} and 488 cm^{-1}, attributed to the SiO_2 component in the composite [31, 32], indicating the incorporation of silica nanoparticles.

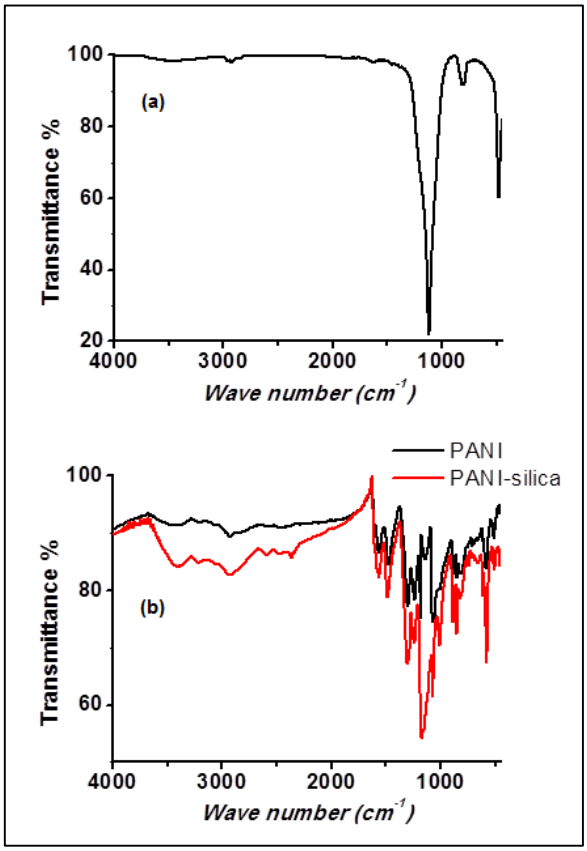

Figure 4 FTIR Spectra of (a) Silica nanoparticles, (b) PANI, and (c) PANI/silica composite.

The XRD pattern of a substance is like fingerprint of the substance and simple tool to test stability of the compound. The X-ray diffraction patterns of the PANI, silica nanoparticles, PANI/silica is illustrated in Fig. 5, variation of the peak intensities against 2θ values. The intense peak at a 25o 2θ value has a similar profile as reported in the literature for polyaniline which indicate that PANI has crystallinity to a certain extent, "semi-crystalline" nature since PANI typically exhibits both crystalline and amorphous regions. This peak may be assigned to the scattering from PANI chains at inter-planar spacing [34, 35]. The X-ray diffraction pattern of silica nanoparticles showed a broad peak appearing at 22° 2θ indicates the amorphous nature of the silica nanoparticles [31]. The X-ray diffraction pattern of PANI/silica showed a peak corresponding to PANI at 25o 2θ value with lower intensity. The reduction in peak intensity at 25° in the composite suggests a change in crystallinity, possibly due to the silica's influence. It would be suggested that the lower intensity may be due to either reduced crystallite size or increased interaction between PANI and the silica, which can disrupt regular packing.

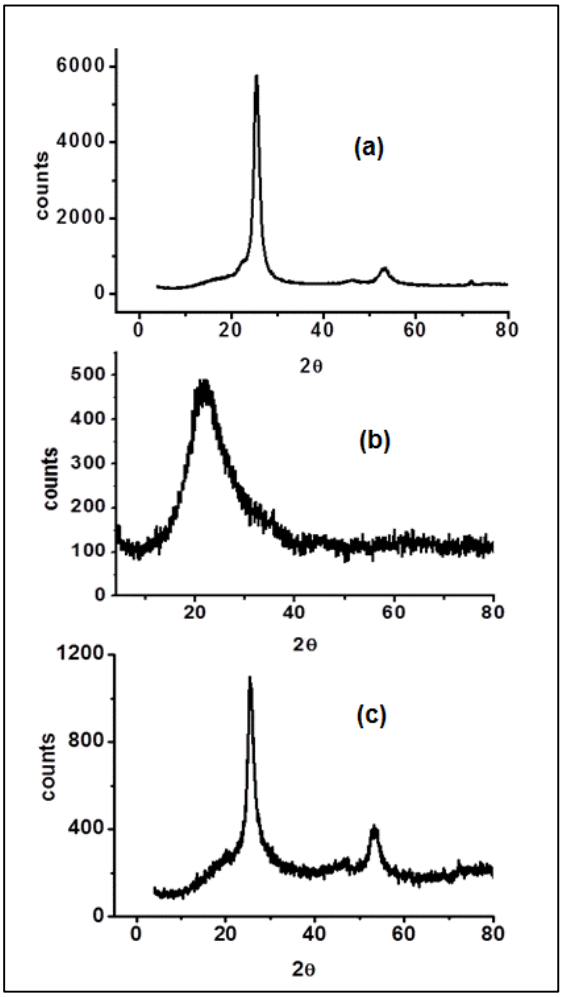

Figure 5 X-ray diffraction pattern of (a) PANI, (b) silica dust particles and (c) PANI/silica composite.

Thermogravimetric analysis (TGA) and differential thermogravimetric (DTG) curves of PANI and PANI/silica are shown in Figure 6. The TGA curve of PANI reveals a three-step weight loss pattern. In the DTG curve, two major minima indicate the primary weight loss stages. The first weight loss, observed around 100°C, is attributed to the loss of absorbed water. The second weight loss, occurring between 100°C and 300°C, is likely due to dopant decomposition. The third weight loss, beginning near 300°C, is associated with the degradation and decomposition of PANI backbone units, leading to the formation of substituted aromatic fragments [36].

The TGA curves of the PANI/silica composite display a two-step weight loss pattern. The third stage, related to the degradation and decomposition of PANI backbone units, is not clearly observed, suggesting enhanced thermal stability of the composite.

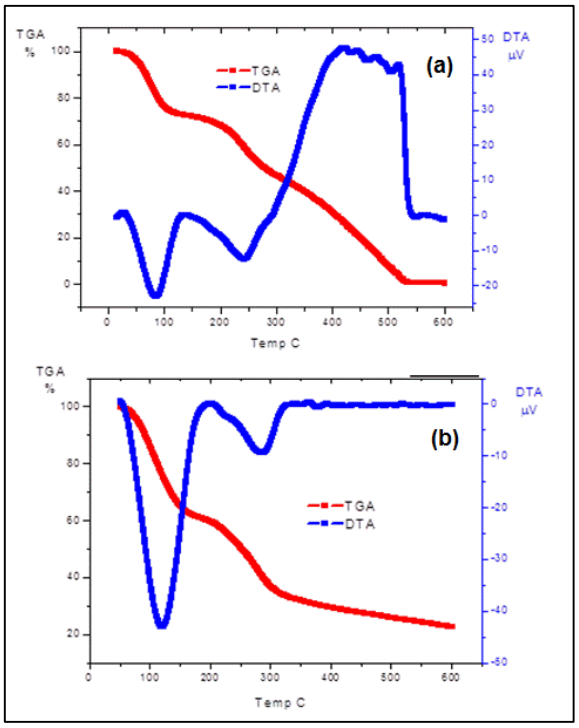

Figure 6 TGA and DTA curves of (a) PANI and (b) PANI/silica composite.

SEM analysis of the PANI layer (Fig. 7a) reveals a grainy, porous structure, with the polymer layer discontinuously covering the stainless steel surface, as previously reported [12, 19]. In the presence of silica nanoparticles, the characteristic grainy structure of the PANI layer changes to a more circular, spongy, or tubular structure, as shown in Fig. 7b.

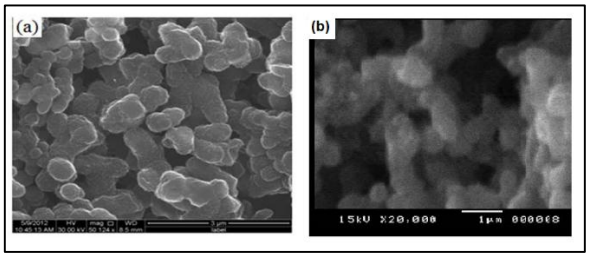

Figure 7 SEM images of (a) PANI and (b) PANI/silica deposited layers.

Protective effects of PANI layers

The main drawback of polymer coatings as protective layers is their significant water absorption, which weakens adhesion and can lead to corrosion of metallic substrates. Therefore, enhancing the protective efficiency of polymer coatings largely depends on reducing WS%. Water sorption was studied over time at two temperatures, 40°C and 70°C. The results show rapid water uptake by the coatings within the first 2-3 hours of immersion, with a higher and faster WS observed at the elevated temperature. Nanocomposites demonstrate a lower water sorption percentage than plain PANI coatings at both 40°C and 70°C. The presence of nanoparticles

consistently reduces WS% in the epoxy matrix [37]. Silica dust particles were found to decrease WS% in PANI by approximately 25% and 5% at 40°C and 70°C, respectively. The nanoparticles form a compact and adherent coating layer, effectively lowering water absorption and providing composites with more stable properties, making them appealing for practical applications.

The underlying oxide layer on the SS electrodes was examined after etching in the etchant solution, as shown in Fig. 8. The surface of bare SS (Fig. 8a) shows severe attack and pitting corrosion due to the aggressive etchant, which penetrates the oxide layer and damages the SS surface. The PANI-doped sulfate composite coating (Fig. 8b) exhibits fewer corrosion pits, with slight improvement in corrosion resistance. Greater improvement is observed in the corrosion resistance of the PANI-doped phosphate composite surface (Fig. 8c), indicating a more protective oxide layer.

In the case of the oxide layer beneath the PANI/silica nanocomposite (Fig. 8d), a compact and adherent oxide forms, providing excellent protection against the etchant. An iron phosphate layer, typically forming on passive SS surfaces due to the phosphate-doped coating, further resists the etchant's aggressive action and offers greater protection than the PANI-doped sulfate coating [19]. Additionally, the nanosilica particles enhance passive oxide layer formation.

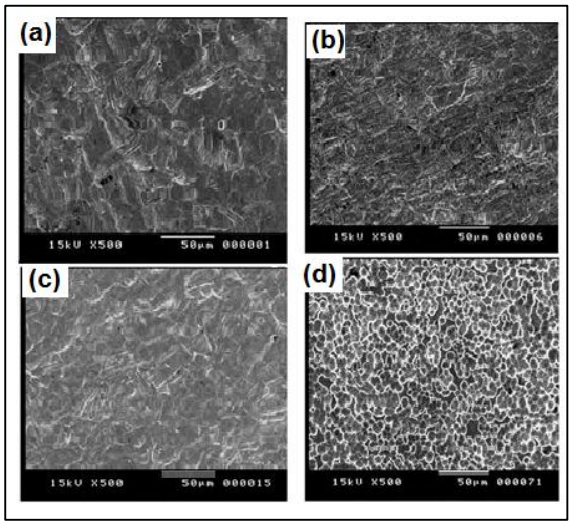

Figure 8 SEM Images – Surface Morphology: Undercoating oxide and after 1-min etching in an etchant solution for (a) bare SS, (b) PANI-sulfate, (c) PANI-phosphate, and (d) PANI composite-phosphate.

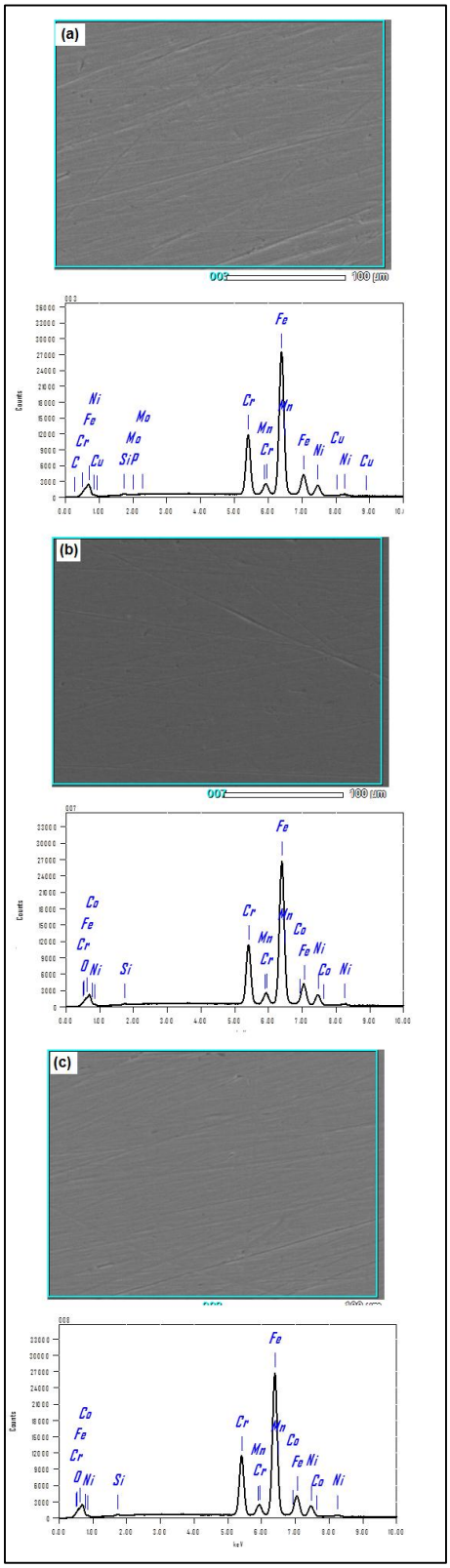

Figure 9 EDX Analysis: Surface characterization of (a) bare SS and underlying coatings of (b) PANI-sulfate and (c) PANI composite-phosphate.

The composition of SS surfaces, after the polymer coatings were removed, was analyzed using EDX, as shown in Fig. 9 and detailed in Table 2. The type of polymer coating has a significant impact on the SS surface composition. Comparison with the uncoated SS composition reveals some notable findings. There is an increase in the amount of chromium, the primary element in the protective

oxide film on SS, particularly in the composite-coated SS samples. A decrease in minor alloying elements, such as C, Mo, and Cu, suggests reduced dissolution of the metal surface [38].

The presence of oxygen in the analysis of phosphate PANI layer coatings indicates an enriched oxide surface. Additionally, an increase in phosphorus in these samples suggests that phosphate anions participate in passive film formation, enhancing the protective oxide layer on SS.

Table 2 EDX analysis (wt.%) of SS surfaces underlying coatings

SS /element	Cr	Mn	Si	Ni	Mo	C	P	Cu	Fe	O
bare SS	18.15	2.23	0.26	8.78	0.08	0.31	0.06	0.25	69.87	0.0
PANI/sulfate	18.32	2.3	0.3	8.56	0.07	0.38	0.03	0.23	69.81	0.0
PANI-phosphate	18.29	2.23	0.28	8.82	0.0	0.0	0.08	0.0	70.08	0.21
PANI/silica-phosphate	18.38	2.18	0.28	8.80	0.0	0.0	0.08	0.0	70.01	0.26

Electrochemical measurements

To determine the optimal amount of silica nanoparticles within the PANI matrix for maximum corrosion protection and adhesion, potential-time measurements were performed for different silica-containing PANI coatings in a 3.5% NaCl solution. All coated SS samples showed a more noble behavior compared to the uncoated sample and maintained passivity (spontaneous passivation) for a defined period before passivity breakdown. Among the coatings, PANI with 0.04 g silica (PANI-0.04 silica) provided the longest duration in the passive region, with no pitting observed beneath the polymer coating after immersion. Incorporating silica into PANI improved protection up to 0.04 g; beyond this concentration, protection declined. Thus, a silica concentration of 0.04 g per 100 mL in the PANI matrix is optimal for sustaining adequate passivity.

Figure 10 shows the open-circuit potential over time for uncoated and PANI/silica-coated SS samples after various aging times in a phosphate solution (doping times of 1–48 hours, three days, and seven days). All coated composites demonstrate a more noble potential compared to the uncoated SS substrate. Aging in phosphate solution prolonged the duration of passivity in chloride solution; for example, the composite with a two-day phosphate doping retained passivity for more than 14 hours. The three-day phosphate-doped composite (Fig. 10b) exhibited some initial fluctuations in the passive region but maintained passivity for over 240 hours. The seven-day phosphate-doped PANI/silica composite (Fig. 10c) achieved outstanding passivity, retaining its protective integrity for more than 350 hours without passivity breakdown. In summary, phosphate-doped PANI/silica coatings aged for more than three days maintained potential in the passive region for an extended period, with no passivity breakdown observed. This suggests they offer an excellent barrier against the diffusion of corrosive chloride ions.

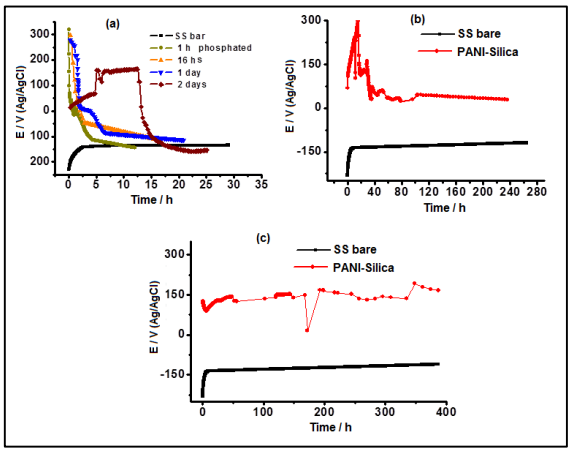

Figure 10 Eocp− time behavior in 3.5% NaCl solution for un-coated, PANI/silica coated SS doped phosphate over (a) 1-48 h, (b) three days and (c) seven days doped phosphate.

The anodic polarization of PANI/silica coatings on steel, doped with phosphate for three and seven days, was performed in a 3.5% NaCl solution at room temperature, and the results were compared to uncoated SS, as shown in Fig. 11. The three-day phosphate-doped coating shows a passivation plateau within the potential range of -349 to 252 mV, a broader passivation range than that of the uncoated SS (Fig. 11a). Additionally, the pitting potential shifts by over 80 mV in the positive direction.

For the seven-day phosphate-doped PANI/silica coating (Fig. 11b), two passivation plateaus are observed: one within the potential range of -215 to 463 mV, with a significantly lower passive current, followed by a higher passive current plateau from -465 to 810 mV. This behavior may be due to the formation of multiple layers of passive oxides or a re-passivation process occurring during anodic polarization. The pitting corrosion potential reaches 830 mV, providing a wider passivation range than uncoated SS, alongside a lower passive current density, indicating effective corrosion protection and a stable passive oxide film. The highly phosphated nanocomposite displays exceptional passivation, as the seven-day phosphated coating maintains its passivity at more positive potentials for an extended period [26, 39].

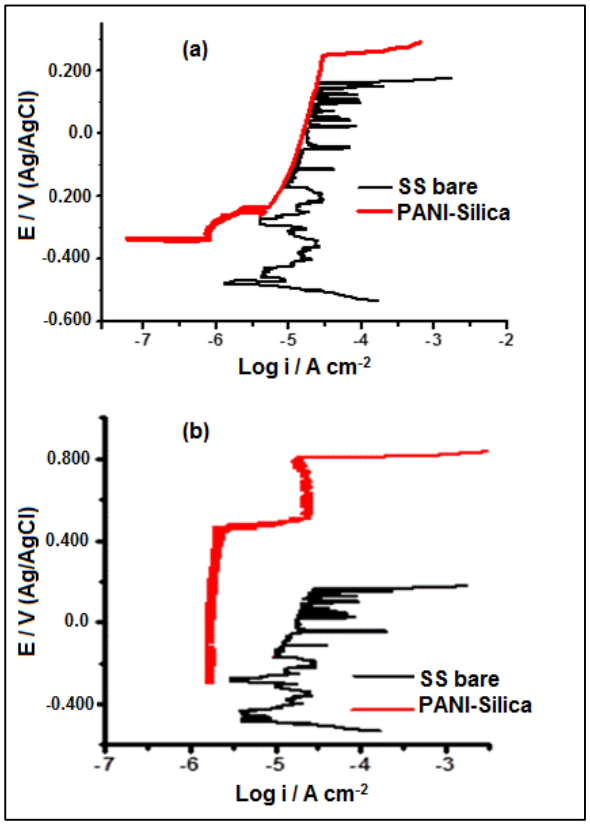

Figure 11 Anodic polarization behavior of PANI/silica-coated SS after (a) 3 days and (b) 7 days of phosphate doping, compared with uncoated SS.

The barrier protection offered by the phosphate-doped coatings likely results from the blocking effect of phosphates, forming a protective metal phosphate layer through reactions between metal cations and released phosphate doping anions [13, 40]. Additionally, the silica nanoparticles hinder electrolyte diffusion by filling micropores within the coating. Another proposed mechanism is that polyaniline induces the oxidation of the metal surface, forming a stable metal oxide layer and maintaining the metal in its passive or "noble" state. For this to occur, the polymer must have a lower oxidation potential than the metal it protects. Since PANI has a lower oxidation potential than SS, it is preferentially oxidized. However, the oxidized form of PANI remains insoluble in the corrosive environment and stays intact on the metal surface, offering prolonged protection.

As PANI acts as an oxidizing agent for leached metal ions, it keeps the metal within the passivation domain by providing a thin protective layer of metal oxide [41]. In addition to barrier protection, the high electrical resistance of the non-conductive polyaniline form (EB) and the presence of silica nanoparticles enhance adhesion to the surface, thereby improving both the physical and functional properties of the coating.

Electrochemical impedance measurements of PANI/silica doped phosphate coated SSs.

EIS measurements were conducted at the corrosion potential (Ecorr) for uncoated SS, PANI-phosphate, and PANI/silica phosphate-coated SS samples at different immersion times in a 3.5% NaCl solution, up to one month. The Nyquist plots are shown in Fig. 12, and all measurements indicate a single capacitive arc or semicircle. The proposed equivalent circuit for these results is illustrated in Fig. 13, where Rs represents the electrolyte resistance, Rc is the coating pore resistance, Rct is the charge transfer resistance, Qc is the constant phase element (CPE) of the coating, and Cdl is the double layer capacitance.

Incorporating the CPE in the equivalent circuit not only minimizes systematic error but also provides detailed insights into the non-ideal dielectric properties of the coating polymer. The estimated parameters are recorded in Table 3. It is evident that the impedance of the coated SS is significantly higher than that of the uncoated SS. As water uptake by the coating increases, the coating capacitance also increases. The coating capacitance of PANI/silica is lower than that of PANI alone, as the nanoparticles reduce water absorption within the PANI, confirming results from water sorption measurements.

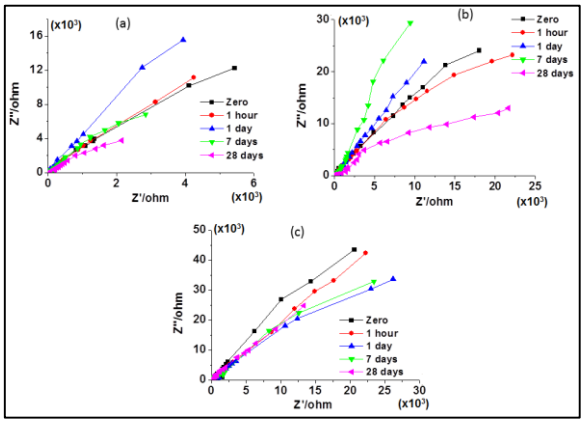

Figure 12 Nyquist plots of (a) un-coated and coated SSs of (b) PANI and (c) PANI/silica seven days doped phosphate in 3.5% NaCl at Ecor.

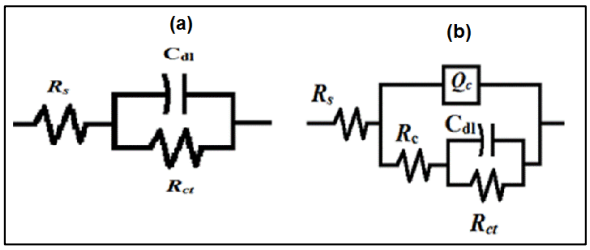

Figure 13 The proposed equivalent circuit of (a) un-coated and (b) coated SSs.

The charge transfer resistance (Rct) value of PANI/silica is high and decreases only slightly over a month of immersion, remaining more than twice that of PANI. This indicates that incorporating silica particles into the PANI layer increases the Rct value over the immersion period. The Rct values for the coated SS samples are much higher than those for uncoated steel, with the silica particles enhancing resistance over time (see Table 3). The PANI/silica-coated steel also shows lower capacitance values (Qc and Cdl) compared to PANI-coated steel during the

initial hours of immersion, although these values increase with prolonged immersion time.

Table 3 the equivalent circuit fitting parameters obtained from the impedance of un-coated and coated SSs at different immersion times in 3.5% NaCl solution.

Time	Sample	R_s (Ω cm^2)	Q_c (Ω^{-1}cm^{-2}S^n)	n	R_c (KΩ cm^2)	C_{dl} (Fcm^{-2})	R_{ct} (KΩ cm^2)
Zero	Bare SS	21.48				1.7E^{-5}	8.90
	PANI	39.2	1.70E^{-5}	0.90	25.55	1.23E^{-5}	53.3
	PANI/silica	45.0	1.16E^{-5}	0.92	75.42	1.13E^{-5}	89.42
1h	Bare SS	20.9				2.23 E^{-5}	19.1
	PANI	40.5	1.96 E^{-5}	0.92	23.25	1.23 E^{-5}	48.15
	PANI/silica	45	1.25 E^{-5}	0.94	67.87	1.24E^{-5}	87.61
1d	Bare SS	21.35				1.58 E^{-5}	31.1
	PANI	37	1.28 E^{-5}	0.91	29.51	1.04 E^{-5}	59.05
	PANI/silica	46	1.87 E^{-5}	1	52.54	1.74 E^{-5}	86.16
10d	Bare SS	27.23				1.48E^{-5}	13.7
	PANI	38	2.18 E^{-5}	0.88	31.28	1.47 E^{-5}	58.47
	PANI/silica	46	4.15 E^{-5}	0.93	46.13	3.25 E^{-5}	63.75
28d	Bare SS	24.09				1.87 E^{-5}	5.68
	PANI	41	1.38 E^{-5}	0.92	26.79	1.37 E^{-5}	48.21
	PANI/silica	43	3.32 E^{-5}	0.84	62.86	2.81 E^{-5}	69.50

The coating and charge transfer resistances, collectively known as polarization resistance (the sum of both resistances), are inversely proportional to the corrosion rate. Higher resistance values indicate a more challenging environment for the corrosion reaction, resulting in a lower corrosion rate. The coating and charge transfer resistances of the nanocomposite are higher than those of the PANI coating, attributing to the enhanced protection of the composite.

Additionally, the doped phosphate anions significantly reduce both types of capacitances (Qcoat and Cdl) while effectively increasing the coating and charge transfer resistances (at the surface-polymer interface), thereby significantly enhancing corrosion resistance. Phosphate doping anions improve corrosion protection by reacting with Fe^{2+} cations to form a protective, undercoated iron phosphate layer [42, 43]. Other metal ions in SS, such as Cr and Ni, may also participate with iron ions in forming an insoluble phosphate layer.

Aging in phosphate has a notable effect on the protective capabilities of the composite coating, with the seven-day phosphate-doped coating demonstrating the highest corrosion resistance. This improvement is due to the enhanced protective surface oxide layer on the steel, a continuous redox reaction within the PANI matrix that helps maintain the passive state of the SS [20], and the possible formation of an additional protective iron phosphate layer [41].

Conclusions

PANI and PANI/silica nanocomposite coatings on stainless steel were electrochemically synthesized from an aqueous acidic solution. The incorporation of silica nanoparticles reduces the electropolymerization rate, but results in thinner, more adherent layers with lower water sorption. The nanoparticles effectively enhance the PANI coating layer, improving passivation of stainless steel in 3.5% NaCl solution. Phosphate ion doping significantly increases the protective efficiency of both PANI and PANI composite coatings, contributing to a dense underlying metal phosphate layer and excellent passive oxide formation. Polyaniline (PANI) and its composites show great promise as protective coatings for corrosion control of steel materials.

Funding Sources

Not available.

Conflicts of Interest

There are no conflicts to declare.

References

[1] Sathiyanarayanan, S., Karpakam, V., Kamaraj, K., Uthukrishnan, S., & Venkatachari, G. (2010). Sulphonate doped polyaniline containing coatings for corrosion protection of iron. Surface and Coatings Technology, 204(7), 1426. https://doi.org/10.1016/j.surfcoat.2009.11.040

[2] Zhu, J., Fan, Z., & Xu, L. (2020). On the propagation of a single pit in stainless steel. Applied Surface Science, 511, 145624. https://doi.org/10.1016/j.apsusc.2020.145624

[3] Hermas, A., Wu, Z. X., Nakayama, M., & Ogura, K. (2006). Passivation of stainless steel by coating with poly(o-phenylenediamine) conductive polymer. Journal of The Electrochemical Society, 153(1), 199. https://doi.org/10.1149/1.2138790

[4] Hermas, A. A., Nakayama, M., & Ogura, K. (2005). Formation of stable passive film on stainless steel by electrochemical deposition of polypyrrole. Electrochimica Acta, 50(17), 3640. https://doi.org/10.1016/j.electacta.2005.03.085

[5] Ozyilmaz, A. T., Ozyilmaz, G., & Yigitoglu, O. (2010). Synthesis and characterization of poly(aniline) and poly(o-anisidine) films in sulphamic acid solution and their anticorrosion properties. Progress in Organic Coatings, 67(1), 28. https://doi.org/10.1016/j.porgcoat.2009.12.007

[6] Singh, T., & Bhargava, A. (2023). Polyaniline/TiO_2 nanocomposite coatings for marine corrosion protection. Journal of Applied Polymer Science, 140(5), 1275–1286. https://doi.org/10.1002/app.52743

[7] Armelin, E., Aleman, C., & Iribarren, J. I. (2009). Anticorrosion performances of epoxy coatings modified with polyaniline: A comparison between the emeraldine base and salt forms. Progress in Organic Coatings, 65(1), 88. https://doi.org/10.1016/j.porgcoat.2008.12.009

[8] Patel, R., Sharma, H., & Singh, S. N. (2024). Conductive carbon nanotube/polyaniline coatings for corrosion inhibition on copper alloys. RSC

Advances, 14(1), 221–234. https://doi.org/10.1039/D3RA06556K

[9] Fuseini, M., Mahmoud, M., Zaghloul, Y., Elkady, M. F., & El-Shazly, A. H. (2022). Evaluation of synthesized polyaniline nanofibers as corrosion protection film coating on copper substrate by electrophoretic deposition. Journal of Materials Science, 57(10), 6085–6101. https://doi.org/10.1007/s10853-022-07114-4

[10] Xu, J., Zhang, Y., Zhang, D., Tang, Y., & Cang, H. (2015). Electrosynthesis of PAni/PPy coatings doped by phosphotungstate on mild steel and their corrosion resistances. Progress in Organic Coatings, 88, 84. https://doi.org/10.1016/j.porgcoat.2015.04.004

[11] Sathiyanarayanan, S., Muthkrishnan, S., & Venkatachari, G. (2006). Corrosion protection of steel by polyaniline blended coating. Electrochimica Acta, 51(29), 6313. https://doi.org/10.1016/j.electacta.2006.01.016

[12] Hür, E., Bereket, G., & Şahin, Y. (2006). Corrosion inhibition of stainless steel by polyaniline, poly(2-chloroaniline), and poly(aniline-co-2-chloroaniline) in HCl. Progress in Organic Coatings, 57(2), 149. https://doi.org/10.1016/j.porgcoat.2006.01.005

[13] Kalendová, A., Veselý, D., Kohl, M., & Stejskal, J. (2014). Effect of surface treatment of pigment particles with polypyrrole and polyaniline phosphate on their corrosion inhibiting properties in organic coatings. Progress in Organic Coatings, 77, 1465. https://doi.org/10.1016/j.porgcoat.2014.07.007

[14] de Souza, S. (2007). Smart coating based on polyaniline acrylic blend for corrosion protection of different metals. Surface and Coatings Technology, 201(15), 7574. https://doi.org/10.1016/j.surfcoat.2007.03.017

[15] Plesu, N., Ilia, G., Pascariu, A., & Vlase, G. (2006). Preparation, degradation of polyaniline doped with organic phosphorus acids and corrosion essays of polyaniline–acrylic blends. Synthetic Metals, 156(3), 230. https://doi.org/10.1016/j.synthmet.2005.10.045

[16] Gupta, G., Cook, A. B., & Khanna, A. S. (2012). Polyaniline-lignosulfonate/epoxy coating for corrosion protection of AA2024-T3. Corrosion Science, 67, 256. https://doi.org/10.1016/j.corsci.2012.01.007

[17] Adhikari, A., Claesson, P., Pan, J., Leygraf, C., Deıdinaite, A., & Blomberg, E. (2008). Electrochemical behavior and anticorrosion properties of modified polyaniline dispersed in polyvinylacetate coating on carbon steel. Electrochimica Acta, 53(12), 4239. https://doi.org/10.1016/j.electacta.2008.01.053

[18] Gao, Y., Syed, J. A., Lu, H., & Meng, X. (2016). Anti-corrosive performance of electropolymerized phosphomolybdic acid doped PANI coating on 304SS. Applied Surface Science, 360, 389. https://doi.org/10.1016/j.apsusc.2015.10.219

[19] Ganash, A. A., Al-Nowaiser, F. M., Al-Thabaiti, S. A., & Hermas, A. A. (2011). Comparison study for passivation of stainless steel by coating with polyaniline from two different acids. Progress in Organic Coatings, 72(5), 480. https://doi.org/10.1016/j.porgcoat.2011.01.008

[20] Lu, H., Zhou, Y., Vongehr, S., Hu, K., & Meng, X. (2011). Electropolymerization of PANI coating in nitric acid for corrosion protection of 430 SS. Synthetic Metals, 161(13), 1368. https://doi.org/10.1016/j.synthmet.2011.04.014

[21] Ohtsuka, T., Iida, M., & Ueda, M. (2006). Polypyrrole coating doped by molybdo-phosphate anions for corrosion prevention of carbon steels. Journal of Solid-State Electrochemistry, 10(8), 714. https://doi.org/10.1007/s10008-006-0106-2

[22] Sathiyanarayanan, S., Azim, S. S., & Venkatachari, G. (2007). A new corrosion protection coating with polyaniline–TiO2 composite for steel. Electrochimica Acta, 52(7), 2068. https://doi.org/10.1016/j.electacta.2006.08.017

[23] Abaci, S., & Nessark, B. (2015). Characterization and corrosion protection properties of composite material (PANI + TiO2) coatings on A304 stainless steel. Journal of Coating Technology and Research, 12(1), 107. https://doi.org/10.1007/s11998-014-9596-2

[24] Hermas, A. A., Abdel Salam, M., & Al-Juaid, S. S. (2013). In situ electrochemical preparation of multi-walled carbon nanotubes/polyaniline composite on stainless steel. Progress in Organic Coatings, 76(12), 1810. https://doi.org/10.1016/j.porgcoat.2013.07.010

[25] Kumar, A. M., Gasem, Z. M., & Gasem, A. (2015). In situ electrochemical synthesis of polyaniline/f-MWCNT nanocomposite coatings on mild steel for corrosion protection in 3.5% NaCl solution. Progress in Organic Coatings, 78(2), 387. https://doi.org/10.1016/j.porgcoat.2014.10.002

[26] Hermas, A. A., Wahdan, M. H., & Ahmed, E. M. (2020). Phosphate-doped polyaniline/Al2O3 nanocomposite coating for protection of stainless steel. Anti-Corrosion Methods and Materials, 67(4), 491. https://doi.org/10.1108/ACMM-11-2019-2295

[27] Jia, Q. M., Zheng, M., Chen, H. X., & Shen, R. J. (2005). Synthesis and characterization of polyurethane/epoxy interpenetrating network nanocomposites with organoclays. Polymer Bulletin, 54(1), 65. https://doi.org/10.1007/s00289-005-0479-6

[28] Ozyılmaz, A. T., Erbil, M., & Yazici, B. (2006). The electrochemical synthesis of polyaniline on stainless steel and its corrosion performance. Current Applied Physics, 6(1), 1. https://doi.org/10.1016/j.cap.2005.07.021

[29] Moraes, S. R., Huerta-Vilca, D., & Motheo, A. J. (2003). Corrosion protection of stainless steel by polyaniline electrosynthesized from phosphate buffer solutions. Progress in Organic Coatings, 48(1), 28. https://doi.org/10.1016/S0300-9440(03)00052-9

[30] Sathiyanarayanan, S., Devi, S., & Venkatachari, G. (2006). Corrosion protection of stainless steel by electropolymerized PANI coating. Progress in

Organic Coatings, 56(2), 114. https://doi.org/10.1016/j.porgcoat.2006.01.01

[31] Huang, K. Y., Weng, C. J., Yeh, J. M., & Chou, T. L. (2009). Preparation and anticorrosive properties of hybrid coatings based on epoxy-silica hybrid materials. Journal of Applied Polymer Science, 112(4), 1933. https://doi.org/10.1002/app.29699

[32] Bagheri, H., & Roostaie, A. (2012). Aniline–silica nanocomposite as a novel solid phase microextraction fiber coating. Journal of Chromatography A, 1238, 22. https://doi.org/10.1016/j.chroma.2012.02.032

[33] Sazou, D., & Georgolios, C. (1997). Formation of conducting polyaniline coatings on iron surfaces by electropolymerization of aniline in aqueous solutions. Journal of Electroanalytical Chemistry, 429(1), 81. https://doi.org/10.1016/S0022-0728(97)00253-X

[34] Wang, S., Tan, Z., Li, Y., Sun, L., & Zhang, T. (2006). Synthesis, characterization, and thermal analysis of polyaniline/ZrO2 composites. Thermochimica Acta, 441(1), 191. https://doi.org/10.1016/j.tca.2005.12.001

[35] Gospodinova, N., & Terlemezyan, L. (1998). Conducting polymers prepared by oxidative polymerization: Polyaniline. Progress in Polymer Science, 23(10), 1443. https://doi.org/10.1016/S0079-6700(98)00030-1

[36] Kumar, A., Kumar, A., Mudila, H., Awasthi, K., & Kumar, V. (2020). Synthesis and thermal analysis of polyaniline (PANI). Journal of Physics: Conference Series, 1531(1), 012108. https://doi.org/10.1088/1742-6596/1531/1/012108

[37] Asiri, A. M., Hussein, M. A., Abu-Zied, B. M., & Hermas, A. E. A. (2015). Enhanced coating properties of Ni-La-ferrites/epoxy resin nanocomposites. Polymer Composites, 36(11), 1875. https://doi.org/10.1002/pc.23191

[38] Hermas, A. A. (2008). XPS analysis of the passive film formed on austenitic stainless steel coated with conductive polymer. Corrosion Science, 50(8), 2498. https://doi.org/10.1016/j.corsci.2008.03.021

[39] Ebrahimi, G., Rezaei, F., & Neshat, J. (2017). Investigation on corrosion protection mechanism of polyaniline nanoparticles doped with phosphoric acid by scanning Kelvin probe and other electrochemical methods. Journal of the Taiwan Institute of Chemical Engineers, 70, 427. https://doi.org/10.1016/j.jtice.2016.10.010

[40] Syed, J. A., Tang, S., & Meng, X. (2016). Intelligent saline enabled self-healing of multilayer coatings and its optimization to achieve redox catalytically provoked anti-corrosion ability. Applied Surface Science, 383, 177. https://doi.org/10.1016/j.apsusc.2016.06.05

[41] Popović, M. M., & Grgur, B. N. (2004). Electrochemical synthesis and corrosion behavior of thin polyaniline-benzoate film on mild steel. Synthetic Metals, 143(2), 191. https://doi.org/10.1016/j.synthmet.2004.05.003

[42] Kinlen, P. J., Ding, Y., & Silverman, D. C. (2002). Corrosion protection of mild steel using sulfonic and phosphonic acid-doped polyanilines. Corrosion, 58(5), 490. https://doi.org/10.5006/1.3278623

[43] Jafarzadeh, P. M. C., Sundell, P.-E., Tyrode, E., & Pan, J. (2016). Active corrosion protection by conductive composites of polyaniline in a UV-cured polyester acrylate coating. Progress in Organic Coatings, 90, 154. https://doi.org/10.1016/j.porgcoat.2015.12.015